FULL PAPER

Stimuli-Responsive Materials

ADVANCED
FUNCTIONAL
MATERIALS

www.afm-journal.de

Efficient Mechanoluminescent Elastomers for Dual-Responsive Anticounterfeiting Device and Stretching/Strain Sensor with Multimode Sensibility

Chen Wu, Songshan Zeng, Zhaofeng Wang,* Fu Wang, Hui Zhou, Jiachi Zhang,* Zhipeng Ci, and Luyi Sun*

In this work, an environmentally friendly and novel oxide-based mechanoluminescent material, $Sr_3Al_2O_6$: Eu^{3+}, which can serve as the alternative for the widely used but environmentally hazardous transition metal–doped sulfides is reported. This oxide could exhibit highly efficient photoluminescence, but even more efficient mechanoluminescence as embedded into polydimethylsiloxane matrix under mechanical stimulation. The emitting color of the resultant $Sr_3Al_2O_6$: Eu^{3+}/polydimethylsiloxane elastomer composites could be further manipulated by adjusting the synthesis atmosphere of the $Sr_3Al_2O_6$: Eu^{3+} based on its unique self-reduction characteristic. Moreover, by combining the wavelength selectivity of photoluminescence and dynamic stress response of mechanoluminescence, $Sr_3Al_2O_6$: Eu^{3+} enables the design of two types of intriguing devices. They are a dual-responsive anticounterfeiting flexible device activated by either photons or mechanics, and a comprehensive stretching/strain sensor capable of sensing both strain level and stretching states. In comparison to the conventional luminescent materials, with a rare combination of efficient photoluminescence, highly sensitive mechanoluminescence, and facile color tunability, $Sr_3Al_2O_6$: Eu^{3+} is much more versatile and ideal for various advanced applications.

1. Introduction

Mechanoluminescence (ML) refers to the phenomenon/process that materials could emit light under mechanical stimuli, e.g., friction, stretch, compression, impact, etc.[1,2] Compared with the conventional photoluminescence (PL) and electroluminescence (EL), ML materials could utilize the ubiquitous mechanical energy in daily life to generate light emissions, avoiding the requirement of an artificial photon- or electron-excitation source. Therefore, ML materials show great advantages in energy saving and environmental protection.[3]

Synthetic ML materials are commonly present in the form of crystals or powders, which can be readily mixed into bulk matrices to generate structural nondestructive ML for practical applications.[4] Among the fabricated composites, elastomer-based ones have attracted increasing attention owing to the rising requirement of incorporating stress-sensing characteristic into the flexible/wearable devices.[5,6] The present ML elastomer composites mainly employ transition metal ion doped sulfides (TM-sulfides) as the luminescent components because of their intense ML intensity.[7,8] However, the TM-sulfides usually have poor chemical stability, and may cause severe environmental pollution as well as lack of rich emission color.[9,10] Theoretically, rare earth doped oxides (RE-oxides) are promising alternatives because of their high chemical stability, nontoxicity, and abundant energy levels.[11] To date, many RE-oxides (such as $SrAl_2O_4$: Eu^{2+},[12,13] $Ca_2Nb_2O_7$: Pr^{3+},[14] $LiNbO_3$: Pr^{3+},[15] $SrMg(PO_4)_2$: Eu^{2+},[16] $CaAl_2Si_2O_8$: Eu^{2+},[17] and $Sr_3Sn_2O_7$: Sm^{3+}[18]) with bright ML have been realized in hard matrices (matrices with Young's modulus typically larger than 1 GPa), while no RE-oxide-based ML elastomer composites were reported due to the lack of complete understanding of the subtle intrinsic mechanism of ML. Therefore, it is essential to develop efficient and ideally multicolored ML of RE-oxide-based elastomer composites, so that flexible devices may possess remarkable and environmentally friendly mechanical responsive optical characteristics.

C. Wu, Prof. Z. Wang, Dr. F. Wang, H. Zhou
State Key Laboratory of Solid Lubrication
Lanzhou Institute of Chemical Physics
Chinese Academy of Sciences
Lanzhou, Gansu 730000, China
E-mail: zhfwang@licp.cas.cn

S. Zeng, Prof. L. Sun
Polymer Program
Institute of Materials Science
and Department of Chemical & Biomolecular Engineering
University of Connecticut
Storrs, CT 06269, USA
E-mail: luyi.sun@uconn.edu

Dr. J. Zhang, Dr. Z. Ci
Department of Materials Science
Lanzhou University
Lanzhou 730000, China
E-mail: zhangjch@lzu.edu.cn

The ORCID identification number(s) for the author(s) of this article can be found under https://doi.org/10.1002/adfm.201803168.

**ADVANCED
SCIENCE NEWS**
www.advancedsciencenews.com

**ADVANCED
FUNCTIONAL
MATERIALS**
www.afm-journal.de

The applications of ML elastomer composites were barely explored until recent years.[19–22] For example, Jeong et al. developed a wind-driven ML device based on a ZnS: Mn^{2+}/Cu^{2+} and polydimethylsiloxane (PDMS) composite.[23] Such a flexible device exhibited bright warm/neutral/cool white light under wind stimulation, potentially applied as a novel environmentally friendly and sustainable lighting system. Wang and co-workers reported a flexible pressure sensor by employing ZnS: Mn^{2+} powders and poly(ethylene terephthalate).[24] By visualizing the dynamic pressure distribution, the pressure sensor was further exploited to be a personalized handwriting device, which could not only record the chirography of signees, but also reflect the writing's physical strength. Like PL and EL materials, ML elastomer composites have potential to fabricate encryption and anticounterfeiting devices as the hidden information could be disclosed under the stimulus of mechanical force.[25,26] However, no specific examples have ever been reported so far. The present applications of ML elastomer composites are mainly focused on the mechanical strength–dependent luminescence or the forms of mechanical behaviors (such as wind, magnetostriction, and electrostriction), while the intrinsic characteristic of ML, that is, the ML can only be generated under a dynamic stress state (such as dynamic stretching), is commonly ignored for developing possible revolutionary applications. While PL has been reported to be able to visualize the static tensile strain level by incorporating the PL materials into soft substrate attached to a rigid light shielding top layer,[27] it is viable to construct a comprehensive sensing system to respond to both strain and stretch state by combining the functionalities of PL and ML with a rational design strategy. This type of intriguing stretching/strain sensor can fit the needs of some artificial intelligent devices for a more comprehensive and dynamic strain-sensing capabilities, while the present research mainly focuses on visualizing static strain level.[28,29]

The previously reported ML of oxides in hard matrices required high loads (usually from 500 to 2000 N) for activation, and the migration of carriers from traps to the conduction band (CB) was considered as the dominant activation mechanism.[12,30] However, for elastomers with low Young's modulus, low force (usually 1–20 N) was applied, which was more difficult to activate the trapped carries as that in hard matrices. $Sr_3Al_2O_6$: Eu^{3+} (SAOE) has been reported to exhibit prominent PL based on the characteristic Eu^{3+}–O^{2-} charge transfer band (CTB; 3.5–6.2 eV) for excitation and f-f transitions of Eu^{3+} for emission.[31] It was reported that SAOE possessed a wide band gap (≈6.3 eV) with relatively deep traps (≈0.3–1.0 eV),[32,33] confirming that there was an energy overlap between Eu^{3+}–O^{2-} CTB and the trapped carriers. Such characteristics provide the possibility for the trapped carriers to be directly transferred to CTB for luminescence, with no need to overcome the energy barrier between traps and CB. This is significant to realize ML in elastomers. Motivated by this consideration, we prepared SAOE powders and investigated their ML behaviors in PDMS elastomers in this work. The results suggest that SAOE could simultaneously emit bright PL and ML as embedded in a flexible PDMS matrix. The luminescent color can be readily tailored on the basis of its distinctive structural self-reduction characteristic. Based on the SAOE/PDMS elastomer composites with both efficient PL and ML, a photonic/mechanical responsive anticounterfeiting device was designed with a concealed pattern that is invisible under daylight and can be revealed under ultraviolet (UV) light source and/or stretched under a dark environment. Furthermore, a smart stretching/strain sensor with a bilayer structure (including a dynamic light shielding top layer) was developed by combining the wavelength selectivity of PL and dynamic stress responsiveness of ML, which could effectively sense both of strain levels and stretching states (e.g., unstretched, dynamic stretching, and stretched to keep a static strain).

2. Results and Discussion

2.1. ML Performance of SAOE/PDMS Composite

The SAOE powders were determined to be single phase of cubic structure with space group of P_a3 (Figure S1, Supporting Information). PDMS was chosen as the elastomer matrix because of its softness/stretchability, ease of fabrication, high optical transparency, and efficient stress transfer ability.[34] The structure of the as-prepared SAOE/PDMS composite is schematically shown in **Figure 1**a. Under the stimuli of rubbing and/or stretching, the SAOE/PDMS composite exhibited intense ML. For definite description, the rubbing and stretching-induced ML are denoted as triboluminescence (TL) and stretch luminescence (SL), respectively. The PL behaviors of the SAOE samples were also investigated for exploring the ML mechanisms (Figure 1b and Figure S2a, Supporting Information). Both PL and ML emissions of SAOE could be attributed to the characteristic f-f transitions of Eu^{3+}.[35] However, the electric-dipole ($^5D_0 \rightarrow {}^7F_2$ at 612 nm) and magnetic-dipole ($^5D_0 \rightarrow {}^7F_1$ at 594 nm) transitions show different behaviors in ML and PL processes (Figure 1b). For PL, the asymmetric ratio ($^5D_0 \rightarrow {}^7F_2$)/($^5D_0 \rightarrow {}^7F_1$) is calculated to be 1.49, which is much higher than that of TL (0.92) and SL (0.86). Such a phenomenon suggests that lattice distortion occurs during ML, since the electric-dipole transition is hypersensitive on the structure symmetry.[36] Both PL and ML show similar doping concentration–dependent luminescent intensity variation (Figure S2, Supporting Information), originating from the competition between radiative and nonradiative transfers of Eu^{3+}.[37]

By comparing the PL and ML spectra of SAOE, one can conclude that their emitting processes both originated from the characteristics f-f transitions of Eu^{3+}. However, the excitation and energy transfer processes of PL and ML are different. To further understand the excitation and energy transfer of ML of SAOE in PDMS elastomers, thermoluminescence (ThL) spectrometer was employed. Figure S3 (Supporting Information) shows the ThL spectra of SAOE under the conditions of before ML, after ML, and after further UV irradiation. The physical information of traps and trapped carriers in the structure could be analyzed based on a classical method (Equations (S1)–(S5), Supporting Information). The corresponding results are presented in Table S1 (Supporting Information). By comparing the trap depths and densities of the trapped carriers before and after ML (Figure 1c), it is evident that nearly all carriers in shallow trap have been released, while deep traps have moved to a shallow position with most of the trapped carriers
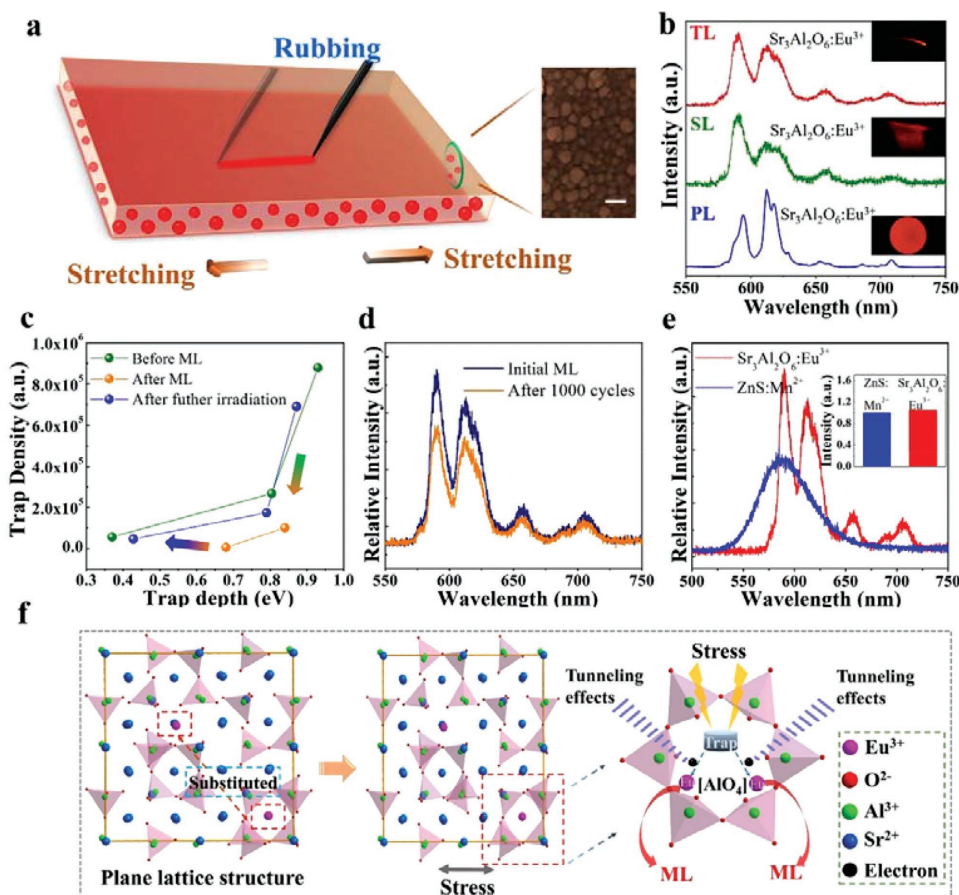
Figure 1. a) Schematic of the ML composite with a cross-section SEM image; scale bar: 50 nm. b) PL, SL, and TL spectral characteristics of $Sr_3Al_2O_6$: 8% Eu^{3+}/PDMS elastomer; insets: luminescent photographs of the corresponding composites. c) Variations of trap depths and carrier densities in $Sr_3Al_2O_6$: 8% Eu^{3+} before ML, after ML, and after further UV irradiation. d) Capacity of ML regeneration of SAOE/PDMS composite after 1000 cycles of stretching. e) Horizontal comparison of the ML performance of the $Sr_3Al_2O_6$: 8% Eu^{3+}/PDMS composite and ZnS: 1.2% Mn^{2+}/PDMS composite; insets: integrated ML intensities. f) Structural illustration of the proposed stress-assisted trap model based on lattice distortion and tunneling processes for ML.

released. Such results provide direct evidence that the release of trapped carriers in the structure should be intrinsically responsible for ML generation. After further irradiating the mechanically stimulated SAOE by a UV lamp, both the trap depths and carrier densities were restored to a great extent, endowing the SAOE/PDMS composite with a capability of ML regeneration. Note that after 1000 cycles of mechanical tests and further UV irradiation, the ML intensity of the SAOE/PDMS composite could maintain ≈90% of the initial value (Figure 1d). To explore the migration paths of the carriers from traps, the ML decay of the SAOE/PDMS composite was measured and plotted as a function of reciprocal intensity (I^{-1}) versus time (t), as shown in Figure S4a (Supporting Information). The nearly linear dependence of I^{-1} versus t suggests that the tunneling-related processes should be responsible for the ML of SAOE in PDMS elastomers, which could avoid the energy barrier between traps and CB.[38] Since there is an energy overlap between Eu^{3+}–O^{2-} CTB (4.05–5.64 eV) and trapped carriers (5.37–5.93 eV) in SAOE, it is suggested that the tunneling transfer of carriers from traps to Eu^{3+}–O^{2-} CTB should be the ML activation mechanism of SAOE. This explains why SAOE could exhibit intense ML even in PDMS elastomers. The electrons in CTB

would then be transferred to the excited energy levels of Eu^{3+}, and finally generate the characteristic emissions of Eu^{3+}. The structural illustration of the ML generation of SAOE in PDMS elastomers based on the lattice distortion and tunneling processes is presented in Figure 1f, and detailed PL and ML mechanisms are depicted in an energy diagram as shown in Figure S4b (Supporting Information).

To estimate the ML efficiency, the $Sr_3Al_2O_6$: Eu^{3+}/PDMS composite was compared with the well-recognized ML material, ZnS: 1.2% Mn^{2+},[39] under the same measuring conditions, e.g., the composition of luminescent powders and PDMS elastomers, stretching conditions, and optical signal collections. It was found that $Sr_3Al_2O_6$: 8% Eu^{3+} exhibits an even higher ML intensity in a PDMS elastomer (≈105%), as shown in Figure 1e. Moreover, SAOE shows much purer red color with color coordinates of ($x = 0.64$, $y = 0.35$; Figure S5, Supporting Information) than that of ZnS: Mn^{2+} ($x = 0.53$, $y = 0.46$).

2.2. ML Color Manipulation

In the structure of $Sr_3Al_2O_6$, europium ions occupy the sites of strontium partially surrounded by AlO_4 tetrahedrons. Under

**ADVANCED
SCIENCE NEWS**
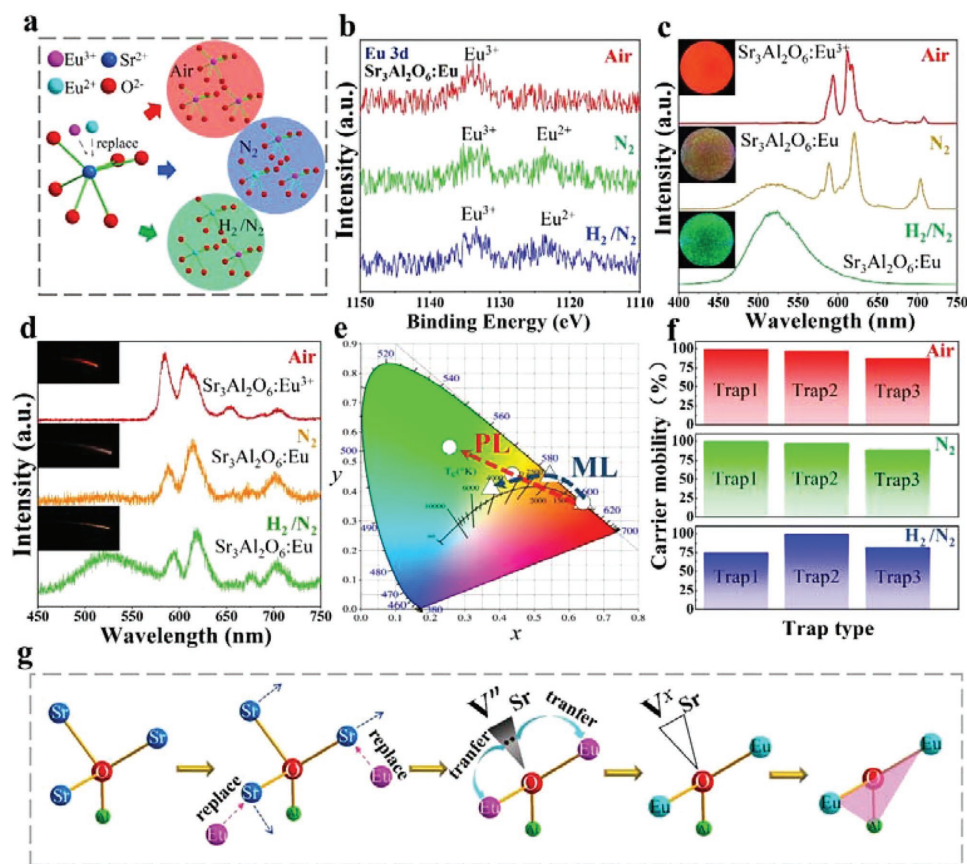www.advancedsciencenews.com

**ADVANCED
FUNCTIONAL
MATERIALS**
www.afm-journal.de

Figure 2. a) Illustration of the form of europium in $Sr_3Al_2O_6$ under air, nitrogen, and nitrogen/hydrogen atmosphere. b) XPS Eu 3d spectra of $Sr_3Al_2O_6$: 8% Eu^{3+} synthesized under different atmospheres. c) PL and d) ML color manipulation of the as-prepared SAOE/PDMS composites based on various Eu^{3+}/Eu^{2+} ratios. e) Color coordinates of the above PL and ML marked on the 1931 CIE diagram. f) Carrier migration abilities of SAOE synthesized under different experimental atmospheres. g) Charge compensation model for the self-reduction of europium in $Sr_3Al_2O_6$.

the experimental condition of air atmosphere, europium is maintained in oxidation state because of the participation of oxygen, exhibiting intrinsic red emission of Eu^{3+}. It is interesting to observe that Eu^{3+} ions could spontaneously reduce to Eu^{2+} under an atmosphere of nitrogen (an inert environment with no oxidation and no reduction), which is called self-reduction (**Figure 2**a,b). Such a phenomenon is believed to be aroused by interior charge self-regulation owing to the nonequivalent substitutions of Eu^{3+} to Sr^{2+},[36,40] as illustrated in Figure 2g. While the previous reports regarding self-reduction had been performed in air synthetic atmosphere, e.g., Eu^{3+} doped $BaMgSiO_4$,[41] SrB_4O_7,[42] and $Sr_4Al_{14}O_{25}$,[43] the characteristics of nonreduction of Eu^{3+} in air and self-reduction of Eu^{3+} in nitrogen are suggested to be attributed to the deficient shielding effect of AlO_4 tetrahedrons, which allows $Sr_3Al_2O_6$ wide adjustment range of Eu^{3+}/Eu^{2+} ratio. By further introducing the reduction atmosphere of hydrogen during synthesis, more Eu^{3+} ions were reduced to Eu^{2+} ones. Since Eu^{2+} exhibits a characteristic d-f emission band located in blue–green range, color manipulation in both PL (from red to yellow and green) and ML (from red to yellowish white) was demonstrated in Figure 2c–e. The ML of both Eu^{2+} and Eu^{3+} was confirmed to come from the released carriers from traps (Figure 2f; Figure S6 and Table S2, Supporting Information).

2.3. Dual-Responsive Anticounterfeiting Device

In addition to lighting and displays, luminescent materials demonstrate promising applications in anticounterfeiting and encryption.[27,44,45] At present, PL materials are mainly employed as the functional components and multilevel anticounterfeiting is further realized based on the adjustments of PL characteristics (e.g., upconversion, downconversion, phosphorescence, etc.).[46,47] Here, we present a stimulating dual-responsive anticounterfeiting device based on the PL and SL characteristics of SAOE (**Figure 3**). As shown in Figure 3a, the pattern of "ML" was extracted from the cured SAOE/PDMS composite, which was then placed in the uncured PDMS/TiO_2 matrix, followed by the immediate curing of this matrix at 60 °C for 4 h. To visually hide the embedded "ML" pattern, TiO_2 powders were introduced into the device as a background, because it shows the same white color as that of the "ML" pattern under daylight and does not generate interference with the produced PL and ML signals. Under daylight, the "ML" pattern was invisible in the SAOE/TiO_2/PDMS flexible device at either unstretched or stretched states (Figure 3b). However, this hidden pattern could be clearly exhibited when irradiated by a UV light or experiencing a stretch stimulus in dark environment (Figure 3c,d). Compared to the conventional
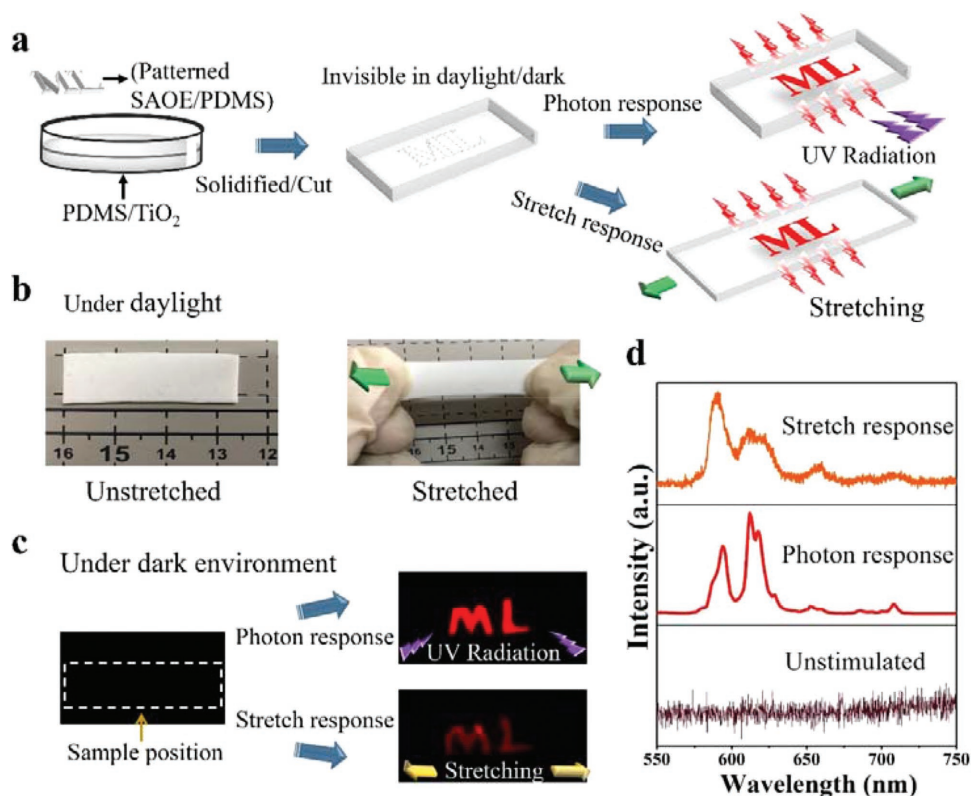
Figure 3. a) Schematic of the fabrication procedures of the dual-responsive anticounterfeiting device. b) Photographs of the device in the conditions of unstretched and stretched under daylight. c) Photon- and stretch-response of the anticounterfeiting device under dark environment. d) Spectra of the device under unstimulated, photon-stimulated, and stretch-stimulated conditions.

anticounterfeiting device made by PL materials responding to only one stimulus, this intriguing dual-responsive anticounterfeiting device activated by both UV radiation and mechanical strain is expected to further elevate the security level of anticounterfeiting technology.

2.4. Stretching/Strain Sensor with Multimode Sensibility

The unique intrinsic characteristic of ML is the dynamic stretch stress responsiveness. In contrast, it is well known that PL is a process independent of stress. If an ML material and a PL material are combined in one elastomer substrate with a rigid light shielding layer atop, there should be no luminescence emitted from the device under an unstretched state. When the device is stretched, a crack opening on the light shielding layer would allow the excitation light to reach the elastomer layer. Thus, as a dynamic stretching is applied, the overall luminescence of the device would come from the combination of ML and PL under the above structural design. While the device is stretched with a static strain, there should be only the luminescence from PL. If the overall emitting color of the combination of ML and PL is distinctively different from the PL only color, it is possible to allow the device to distinguish the stretching states (unstretched, dynamic stretching, and stretched to keep a static strain) and indicate the strain applied on the device. To realize the above design, we made a stretchable device based on an

SAOE/PDMS composite (**Figure 4**a). Here, two kinds of SAOE, one synthesized in air (red emitting) and the other in a nitrogen/hydrogen atmosphere (green emitting), which were denoted as SAOE-R and SAOE-G, respectively, were employed for making the SAOE/PDMS composite. A thin Au layer (≈15 nm in thickness) was sputter coated atop the SAOE/PDMS substrate, which could shield the external UV radiation to the SAOE phosphors at unstretched state. Upon stretching, the light shielding Au layer would be cracked and the opening of the cracks could lead to the activation of the PL underneath (Figure 4b). Once released, the cracks can completely close to re-generate the shielding effect, thus no luminescence can be observed (Figure 4c). To obtain an optimal sensing performance, a UV light of 340 nm was employed as the irradiation source according to the different excitation wavelength selectivity for the PL of SAOE-R (very weak PL excited by 340 nm which can be ignored in this excitation wavelength; Figure S7, Supporting Information) and SAOE-G (strong green PL excited by 340 nm and become the dominating PL color in this excitation wavelength as combined with SAOE-R; Figure S7, Supporting Information). As the device undergoes a stimulus of dynamic stretching (from the moment of starting stretching to the moment of the device reach the predetermined strain; stretching speed: 60 mm s^{-1}), ML of SAOE-R (red light) and SAOE-G (green light), as well as the PL of SAOE-G (green light) appeared. Therefore, in this case, the device exhibited collective emissions with yellow color (Figure 4d), indicating
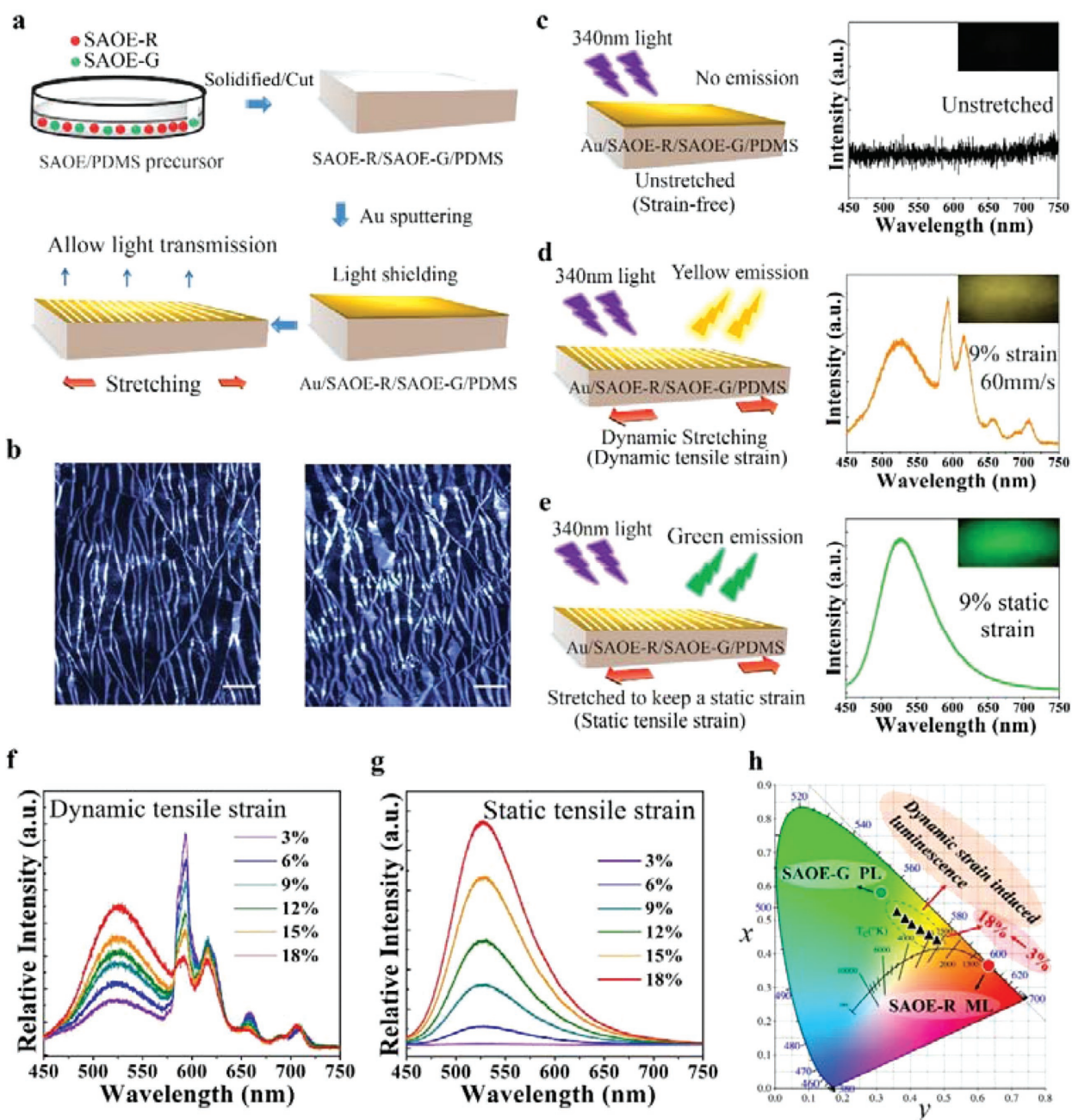
1803168 (5 of 8)

**ADVANCED
SCIENCE NEWS**
www.advancedsciencenews.com

**ADVANCED
FUNCTIONAL
MATERIALS**
www.afm-journal.de

Figure 4. a) Illustration of the fabrication processes of the SAOE/PDMS composite–based stretching/strain sensor with a thin Au light shielding layer. b) Optical microscopic images of crack opening on the Au layer after stretched at a strain of 15% (left) and 30% (right); scale bar: 100 µm. c–e) Schematic structure and corresponding mechanical responsive luminescence of the bi-layered stretching/strain sensor under conditions of unstretched (strain-free), dynamic stretching (dynamic tensile strain: 9%; stretching speed: 60 mm s^{-1}), and stretched to maintain at a static strain (static tensile strain: 9%), respectively. f) Strain-dependent luminescent spectra of the device under a dynamic stretching state. g) Static tensile strain-dependent luminescent spectra of the device; each spectrum was captured after the device reaching the predetermined strain and in a static state. h) Illustration of the emitting color evolution from the dynamic stretching state (combination of the PL of SAOE-G and ML of SAOE-R) to the static tensile strain state (PL of SAOE-G) of the sensor on the 1931 CIE diagram.

the generation of dynamic stretching. If the stretching motion stops but a static strain is maintained on the device, ML of the SAOE disappeared, while the PL of SAOE-G was maintained. As a result, the device showed green light indicating that the device was stretched but kept at a static strain (Figure 4e). The continuous luminescence change of the as-

fabricated stretching/strain sensor from the unstretched state to the states of dynamic stretching and stretched to maintain at a static strain was presented in Movie S1 (Supporting Information).

In addition to effectively sensing the applied stretching states, tensile strain level under different stretching states could be

identified simultaneously. Figure 4f,g shows the tensile strain–dependent luminescent spectra of the bi-layered stretching/strain sensor under the states of dynamic tensile stretching and stretched to maintain at a static strain (static tensile strain), respectively. All spectra were captured by a CCD camera with an integrated time of 0.1 s. Along with the increase of strain, the emission intensity at 524 nm gradually increased regardless of dynamic tensile strain or static tensile strain (Figure S8a, Supporting Information), endowing the device with the ability to specifically determine the strain level. Moreover, the luminescence emitted from the device under dynamic stretching shows gradual color evolution from orange–yellow to green–yellow (Figure 4h) with an increasing tensile strain, allowing the device to sense the dynamic strain level based on the emitting color or the color coordinates (x, y), as shown in the Figure S8b (Supporting Information). Note that the ML intensity of the device under dynamic stretching gradually decreases along with an increase of strain due to the continuous consumption of trapped electrons in structure (Figure 4f); the sensing of dynamic stretching state and strain level responses in this bi-layered sensor are valid when the strain is below 18%. A wider strain variation range can be easily achieved by employing an elastomer matrix with a higher stretchability. The as-fabricated SAOE/PDMS composite–based stretching/strain sensor with multimode sensibility shows promising application prospects in mechanical failure monitoring, intelligent artificial skin, and other related fields.

3. Conclusion

In summary, we have developed SAOE/PDMS composites with intense ML, whose intensity is even higher than that of ZnS: Mn^{2+}. The variation of site symmetry of luminescent centers as well as the carrier migration from traps stimulated by stress provides direct evidence for the ML mechanisms. The unique lattice structure endows SAOE with the ability of self-reduction, and therefore color manipulation was easily realized by adjusting the reaction atmosphere. Based on the PL and ML performance of the SAOE/PDMS composite, a dual-responsive anticounterfeiting device was fabricated. Furthermore, by combining the wavelength selectivity of PL and dynamic tensile stress responsiveness of ML, an unprecedented stretching/strain sensor was developed which could sense the stretching states and strain level simultaneously, showing promising applications in mechanical failure monitoring, intelligent artificial skin, and other related fields.

Supporting Information

Supporting Information is available from the Wiley Online Library or from the author.

Conflict of Interest

The authors declare no conflict of interest.

[1] X. Wang, C. N. Xu, H. Yamada, K. Nishikubo, X. G. Zheng, *Adv. Mater.* **2005**, *17*, 1254.
[2] D. Tu, C.-N. Xu, Y. Fujio, A. Yoshida, *Light: Sci. Appl.* **2015**, *4*, e356.
[3] S. M. Jeong, S. Song, H. Kim, *Nano Energy* **2016**, *21*, 154.
[4] D. Peng, B. Chen, F. Wang, *ChemPlusChem* **2015**, *80*, 1209.
[5] X. Wang, M. Que, M. Chen, X. Han, X. Li, C. Pan, Z. L. Wang, *Adv. Mater.* **2017**, *29*, 1605817.
[6] H. Zhang, D. Peng, W. Wang, L. Dong, C. Pan, *J. Phys. Chem. C* **2015**, *119*, 28136.
[7] S. M. Jeong, S. Song, S.-K. Lee, B. Choi, *Appl. Phys. Lett.* **2013**, *102*, 051110.
[8] S. M. Jeong, S. Song, S.-K. Lee, N. Y. Ha, *Adv. Mater.* **2013**, *25*, 6194.
[9] W. Xiao, F. Lei, Y. Yin, L. Shi, J. Xie, L. Zhang, *Solid State Sci.* **2017**, *72*, 116.
[10] H. Zhu, M. Fang, Z. Huang, Y. Liu, K. Chen, Y. Min, Y. Mao, M. Wang, *J. Lumin.* **2016**, *172*, 180.
[11] M. J. Dejneka, A. Streltsov, S. Pal, A. G. Frutos, C. L. Powell, K. Yost, P. K. Yuen, U. Müller, J. Lahiri, *Proc. Natl. Acad. Sci. USA* **2003**, *100*, 389.
[12] C.-N. Xu, T. Watanabe, M. Akiyama, X.-G. Zheng, *Appl. Phys. Lett.* **1999**, *74*, 2414.
[13] K.-S. Sohn, M. Y. Cho, M. Kim, J. S. Kim, *Opt. Express* **2015**, *23*, 6073.
[14] J.-C. Zhang, Y.-Z. Long, X. Yan, X. Wang, F. Wang, *Chem. Mater.* **2016**, *28*, 4052.
[15] D. Tu, C.-N. Xu, A. Yoshida, M. Fujihala, J. Hirotsu, X.-G. Zheng, *Adv. Mater.* **2017**, *29*, 1606914.
[16] S. Kamimura, H. Yamada, C.-N. Xu, *J. Lumin.* **2012**, *132*, 526.
[17] L. Zhang, H. Yamada, Y. Imai, C.-N. Xu, *J. Electrochem. Soc.* **2008**, *155*, J63.
[18] S. Kamimura, H. Yamada, C.-N. Xu, *Appl. Phys. Lett.* **2012**, *101*, 091113.
[19] Y. Zhang, G. Gao, H. L. W. Chan, J. Dai, Y. Wang, J. Hao, *Adv. Mater.* **2012**, *24*, 1729.
[20] M.-C. Wong, L. Chen, M.-K. Tsang, Y. Zhang, J. Hao, *Adv. Mater.* **2015**, *27*, 4488.
[21] H. Fang, X. Wang, Q. Li, D. Peng, Q. Yan, C. Pan, *Adv. Energy Mater.* **2016**, *6*, 1600829.
[22] J. S. Kim, G.-W. Kim, *Sens. Actuators, A* **2014**, *218*, 125.
[23] S. M. Jeong, S. Song, K.-I. Joo, J. Kim, S.-H. Hwang, J. Jeong, H. Kim, *Energy Environ. Sci.* **2014**, *7*, 3338.
[24] X. Wang, H. Zhang, R. Yu, L. Dong, D. Peng, A. Zhang, Y. Zhang, H. Liu, C. Pan, Z. L. Wang, *Adv. Mater.* **2015**, *27*, 2324.
[25] L. Chen, M.-C. Wong, G. Bai, W. Jie, J. Hao, *Nano Energy* **2015**, *14*, 372.

**ADVANCED
SCIENCE NEWS**

www.advancedsciencenews.com

**ADVANCED
FUNCTIONAL
MATERIALS**

www.afm-journal.de

[26] Z. Song, R. Liu, Y. Li, H. Shi, J. Hu, X. Cai, H. Zhu, *J. Mater. Chem. C* **2016**, *4*, 2553.

[27] S. Zeng, D. Zhang, W. Huang, Z. Wang, S. G. Freire, X. Yu, A. T. Smith, E. Y. Huang, H. Nguon, L. Sun, *Nat. Commun.* **2016**, *7*, 11802.

[28] M. Amjadi, A. Pichitpajongkit, S. Lee, S. Ryu, I. Park, *ACS Nano* **2014**, *8*, 5154.

[29] K. K. Kim, S. Hong, H. M. Cho, J. Lee, Y. D. Suh, J. Ham, S. H. Ko, *Nano Lett.* **2015**, *15*, 5240.

[30] J.-C. Zhang, Y. Wan, X. Xin, W.-P. Han, H.-D. Zhang, B. Sun, Y.-Z. Long, X. Wang, *Opt. Mater. Express* **2014**, *4*, 2300.

[31] Y. Pan, H. H. Y. Sung, H. Wu, J. Wang, X. Yang, M. Wu, Q. Su, *Mater. Res. Bull.* **2006**, *41*, 225.

[32] M. Akiyama, C.-N. Xu, M. Taira, K. Nonaka, T. Watanabe, *Philos. Mag. Lett.* **1999**, *79*, 735.

[33] S. K. Sharma, S. S. Pitale, M. M. Malik, M. S. Qureshi, R. N. Dubey, *J. Alloys Compd.* **2009**, *482*, 468.

[34] S. M. Jeong, S. Song, H. Kim, K.-I. Joo, H. Takezoe, *Adv. Funct. Mater.* **2016**, *26*, 4848.

[35] D. Kumar, K. G. Cho, Z. Chen, V. Craciun, P. H. Holloway, R. K. Singh, *Phys. Rev. B* **1999**, *60*, 13331.

[36] S. Som, A. K. Kunti, V. Kumar, V. Kumar, S. Dutta, M. Chowdhury, S. K. Sharma, J. J. Terblans, H. C. Swart, *J. Appl. Phys.* **2014**, *115*, 193101.

[37] Z. Wang, Y. Li, Q. Jiang, H. Zeng, Z. Ci, L. Sun, *J. Mater. Chem. C* **2014**, *2*, 4495.

[38] Z. Pan, Y.-Y. Lu, F. Liu, *Nat. Mater.* **2011**, *11*, 58.

[39] D. O. Olawale, T. Dickens, W. G. Sullivan, O. I. Okoli, J. O. Sobanjo, B. Wang, *J. Lumin.* **2011**, *131*, 1407.

[40] B. Liu, Y. Wang, J. Zhou, F. Zhang, Z. Wang, *J. Appl. Phys.* **2009**, *106*, 053102.

[41] M. Peng, Z. Pei, G. Hong, Q. Su, *J. Mater. Chem.* **2003**, *13*, 1202.

[42] Z. Pei, Q. Su, J. Zhang, *J. Alloys Compd.* **1993**, *198*, 51.

[43] M. Peng, N. Da, Y. Qiao, B. Wu, C. Wang, D. Chen, J. Qiu, *J. Rare Earths* **2006**, *24*, 749.

[44] C. Zhang, B. Wang, W. Li, S. Huang, L. Kong, Z. Li, L. Li, *Nat. Commun.* **2017**, *8*, 1138.

[45] X. Li, Y. Xie, B. Song, H.-L. Zhang, H. Chen, H. Cai, W. Liu, Y. Tang, *Angew. Chem., Int. Ed.* **2017**, *129*, 2733.

[46] X. Liu, Y. Wang, X. Li, Z. Yi, R. Deng, L. Liang, X. Xie, D. T. B. Loong, S. Song, D. Fan, A. H. All, H. Zhang, L. Huang, X. Liu, *Nat. Commun.* **2017**, *8*, 899.

[47] Y. Liu, K. Ai, L. Lu, *Nanoscale* **2011**, *3*, 4804.

1803168 (8 of 8)